*Proceedings of International Symposium on Bond Behaviour of FRP in Structures (BBFS 2005)*
*Chen and Teng (eds)*


# SIMULATION OF BOND FAILURE IN RC BEAMS STRENGTHENED WITH FRP SHEETS SUBJECTED TO DYNAMIC/IMPACT LOADINGS

S. Mohammadi [1], A.A. Mousavi Khandan [2]
[1] Department of Civil Engineering, University of Tehran, Tehran, Iran
Tel: +98-21-6111 2258, Fax:+98-21-6403808, Email: smoham@ut.ac.ir
[2] Department of Civil Engineering, University of Tehran, Tehran, Iran

## ABSTRACT

This paper presents a combined finite/ discrete element method for 2D and 3D modelings of strengthened RC beams subjected to dynamic/impact loadings. The main task is set on developing an algorithm for simulation of potential bonding and debonding/delamination phenomena during impact or general dynamic loading conditions. The proposed approach adopts a general node to face nonlinear frictional contact algorithm to enforce the bonding/debonding constraints between concrete and FRP. Parameters required by the contact mechanics procedures are determined from the bonding properties. Furthermore, a bilinear softening model for adhesive layer coupled with a mixed mode fracture model has been utilized. The validity of developed algorithm is verified with available experimental and numerical benchmarks.

## KEYWORDS

FRP, RC beams, strengthening, interfacial stresses, impact loading, debonding.

## INTRODUCTION

Structures are subject to various types of damage in their life time, induced by either loads higher than the design service loads, or by chemical processes due to aggressive environmental conditions. FRP composites have been widely used for repair and retrofitting purposes and provide unique advantages in comparison to the conventional steel bars/plates, such as high strength-to-weight ratio and good resistance to corrosion. Plate bonding for structural strengthening was utilized in the early 1960's and was later widely used worldwide ( Klaiber et al. (1987), Lander et al. (1981)). Miere (1978) adopted the technique of applying fiber reinforced polymer (FRP) sheets to the tensile face of reinforced concrete (RC) beams for flexural strengthening.
There have been many attempts for numerical simulation of concrete beams strengthened by FRP composites. (Zhang et al. 1997, Ziraba 1995, Arduini et al. 1995, Jerome et al. 1997, Rahimi et al. 2001). Complexity of the problem and the interaction of different interfaces between concrete, steel, FRP plate and adhesive layer have so far left little success in simulating debonding failures under dynamic loads. Another essential part of the simulation is the bonding/ debonding behavior of the adhesive layer. Taljesten theoretically derived a linear equation for calculating the load carrying capacity of a FRP-bonded concrete. Yaun et al. (2001) and Nishida et al. (1999) also proposed alternative types of nonlinear ($\tau$-$\delta_t$) relationships.
By examining the results of a wide range of experimental tests, debonding failures in flexurally strengthened RC beams may be classified into two types: end debonding, in which failure starts from one end of the plate due to local stress concentration, and intermediate crack induced debonding in which debonding starts from either a flexural crack or a flexural shear crack (Teng et al. 2002).
Figure 1 illustrates different failure modes of a typical concrete beam strengthened by a FRP plate. In case of the cover separation failure mode, where the bond strength of adhesive layer is relatively high, microdiagonal cracks that occur in the interfacial concrete finally connect together and lead to the delamination of FRP sheets as depicted in Figure 1b. In case of weak or imperfect bond, the debonding may happen within the epoxy adhesive layer (Figure 1a). In both cases, a flexural crack locally occurs at mid span from which the debonding initiates and propagates. The third major type of debonding is schematically shown in Figure 1c, in which a secondary diagonal shear or flexural crack occurs beside the first flexural concrete crack at mid span. Then, the debonding starts to propagate from the root of the secondary diagonally shear or flexural crack.
In this study, a new approach based on the combined finite/discrete element method has been developed. The proposed algorithm consists of full material and geometry non-linearities. An “explicit central difference time

integration technique" is adopted in order to increase the computational efficiency, especially for impact simulations. The present discrete element method, utilizes the principles of penalty based contact mechanics in order to enforce evolving contact constraints. The use of discrete elements in problems with evolving geometry and boundary conditions in successive time steps, combined with its capability of error estimation and adaptive remeshing, provides us with a powerful numerical tool for modeling complex problems (Mohammadi 2003). Bonding/debonding behavior of FRP-concrete interface is modeled by a mixed mode model based on the Hashin criterion with a bilinear strain softening model. For 3D problems, mixed mode debonding model has been developed for FRP-concrete interface.

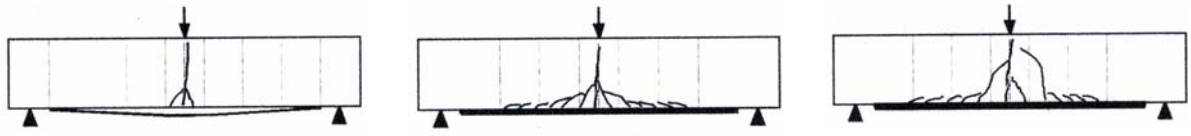

a) weak/imperfect bond b) cover separation c) diagonal cracking

Figure1. Interfacial debonding failure mode (Zhishen et al. 2003).

## MATERIAL MODELING

### Concrete and CFRP Material Models

A Drucker-Prager material model within an associated flow rule of plasticity is used for modeling the compressive behavior of concrete. The Rankine fracture model is utilized to model the tensile behaviour of concrete while a bilinear strain softening law is adopted to ensure a smooth non-local release of fracture energy. On the other hand, no rupture in CFRP sheets has been reported in experimental tests (Jerome et al. 1997). As a result, the behavior of CFRP is assumed to be orthotropic linear elastic till their tensile strength.

### Material Model for FRP-Concrete Interface

Debonding in FRP-concrete interface is one of the major failure modes in strengthened RC beams. In the proposed algorithm, a 3D Hashin model is adopted to predict initiation of interfacial debonding. Beginning with the assumption of large deformations, the rate of the Green-Lagrange strain tensor is decomposed into elastic and inelastic parts. The inelastic strain rate follows the associated flow rule:

$$\dot{\bar{E}} = \dot{\bar{E}}^{el} + \dot{\bar{E}}^{in} \tag{1}$$

$$\dot{\bar{E}}^{el} = \bar{C}\dot{\bar{S}}\ , \quad \dot{\bar{E}}^{in} = \dot{\bar{E}}^{pl} = \dot{\lambda}\frac{\delta F}{\delta \bar{S}} \tag{2}$$

Here, $\bar{C}$ is the elasticity matrix for plane isotropic behavior of the material. $\bar{S}$ is the stress matrix, $\lambda$ is the inelastic coefficient and F is the yield function. The Hashin delamination criterion is a function of interlaminar stresses $\bar{S}^{33}, \bar{S}^{13}, \bar{S}^{23}$, tensile strength in direction of the thickness $Z_0$ and tangential strength of layer $R_0$.

$$\frac{\left(\bar{S}^{33}\right)^2}{{Z_o}^2} + \frac{\left(\bar{S}^{13}\right)^2 + \left(\bar{S}^{23}\right)^2}{{R_o}^2} \le 1 \tag{3}$$

The yield function $F(\bar{S},\alpha)$ is defined from the delamination criterion and a linear softening function $Z(\alpha)$ :

$$F\left(\bar{S},\alpha\right) = g\left(\bar{S}\right) - Z\left(\alpha\right) \le 0, \quad g\left(\bar{S}\right) = \sqrt{\bar{S}^T A \bar{S}} \tag{4}$$

$$A = \begin{bmatrix} 0 & 0 & 0 & 0 & 0 & 0 \\ 0 & 0 & 0 & 0 & 0 & 0 \\ 0 & 0 & 1 & 0 & 0 & 0 \\ 0 & 0 & 0 & 0 & 0 & 0 \\ 0 & 0 & 0 & 0 & \left(\frac{Z_o}{R_o}\right)^2 & 0 \\ 0 & 0 & 0 & 0 & 0 & \left(\frac{Z_o}{R_o}\right)^2 \end{bmatrix} \tag{5}$$

$$Z\left(\alpha\right) = Z_o\left(1 - \mu\alpha\right) \tag{6}$$

The variable $\alpha$ can be assumed as the equal inelastic strain. The parameter $\mu$ describes the slope of the softening function $Z(\alpha)$. It is a material parameter and can be determined from the critical energy release rate $G_c$, tensile strength $Z_0$ and the thickness of the intermediate layer $h_T$:

$$\mu = \frac{Z_o \times h_T}{2G_c} \tag{7}$$

The rate of the internal variable is defined with the evolution law:

$$\dot{\alpha} = -\dot{\lambda}\frac{\partial F}{\partial Z} \tag{8}$$

The gradient of the yield function is derived as follows:

$$\frac{\partial F}{\partial \bar{S}} = \frac{1}{g(\bar{s})} A\bar{S} = N,\ \frac{\partial F}{\partial Z} = -1 \tag{9}$$

Using equations (9) and (1-2) and adopting a backward Euler algorithm within a time step $t_{n+1} = t_n + \Delta t$ yields:

$$\bar{E}_{n+1} = \bar{C}^{-1}\bar{S}_{n+1} + \bar{E}_n^{\,pl} + \frac{\lambda}{g(\bar{S}_{n+1})} A\bar{S}_{n+1} \tag{10}$$

$$\bar{S}_{n+1} = \left[\bar{C}^{-1} + \frac{\lambda}{Z(\alpha_{n+1})} A\right]\left[\bar{E}_{n+1} - \bar{E}_n^{\,pl}\right] \tag{11}$$

$$\bar{S}_{n+1} = P\bar{E}^{tr} \tag{12}$$

where subscripts n and n+1 denote the quantities of the known converged configuration at time $t_n$ and $t_{n+1}$, respectively. Updating the internal parameter $\alpha$ is performed using a backward Euler integration:

$$\alpha_{n+1} = \alpha_n + \lambda \tag{13}$$

Linearization of the stress tensor has to be derived for the finite element formulation. After some algebric manipulations we end up with the consistent tangent matrix:

$$\bar{D} = P - \frac{PN(PN)^T}{N^T PN + H},\ H = \frac{Z'}{1 - \lambda\dfrac{Z'}{Z}},\ Z' = -\mu \tag{14}$$

## NUMERICAL SIMULATION

### Concrete Beam Strengthened by CFRP subjected to Impact Loading

A CFRP strengthened RC beam (without internal steel reinforcement), reportedly tested by Jerome & Ross (1997), was analyzed in this study. The dimensions of the simply supported beam were 3×3×30 in (7.62×7.62×76.2 cm). The size of the CFRP panel was 3×30 inch, each composed of three plies. Properties of concrete and CFRP panels are given in Table 1. The drop-weight center-point loadings were conducted with the measured dynamic loading curve versus time as shown in Figure 2.

### 2D Modeling

Because of the symmetry of loading and geometry only one half of the beam was modeled as depicted in Figure 5. Due to lack of information for adhesive material, fracture energy release rate and bond strength are taken 0.5 N/mm and 4 Mpa respectively. Analysis was conducted in a plane stress state with triangular plane stress elements for concrete beam and CFRP sheet (Figure 3). The size of these elements varied due to their distance to CFRP sheet, so those elements adjacent to CFRP sheet had a size of 0.001 m and elements adjacent to top of the beam had a size of 0.01 m. The elements of CFRP sheet had a size of 0.00025 m which was decomposed of two layers of elements through the thickness.

Failing to properly set one of several parameters affecting the results such as contact related parameters, fracture properties and material related data may result in unrealistic results as depicted in Figure 4. Contact penalty coefficient, contact zone, bonding/frictional effects and the size of timestep are among the main contributing parameters affecting the quality of a contact analysis.

According to the report by Jerome et al. (1997) flexural cracks occurred between 400 $\mu s$ till 500 $\mu s$ and by 600 $\mu s$, the cracks ran to the upper surface of the beam, which is in a close agreement with results of the performed

simulation (Figure 5). Test data for a point located on the bottom center of the beam, indicated an abrupt change of slope in the strain-vs-time curve at about 430 $\mu s$, indicating crack initiation has occurred. At the original neutral axis of the beam, failure appeared at about 430 $\mu s$. At another point located at 2.75 inch from the bottom of the beam, a change of slope in strain-time curve is seen at about 555 $\mu s$, indicating the crack(s) reaching the upper surface of the beam. A post-test damage assessment indicated the formation of a single flexural crack at the beam's midpoint. The results show that flexural cracks were propagated at the bottom part of mid span at 460$\mu s$. These flexural cracks started to propagate from two distinct origins very close to mid span. Later, these cracks started to develop to upper surface of the beam in time interval of 460 $\mu s$ to 750 $\mu s$. They reached to top of the beam at 750 $\mu s$.

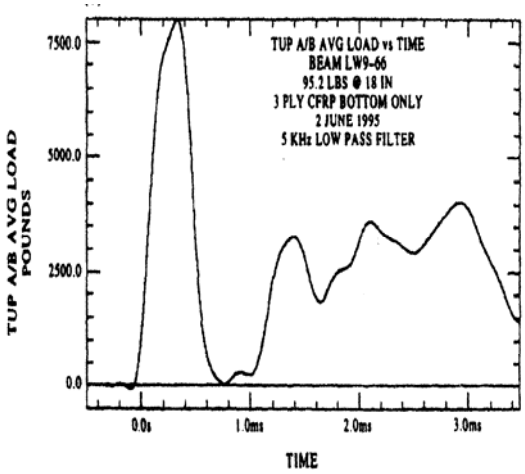


Figure 2. Load-time curve (Jerome et al. 1997)

| Concrete | | CFRP | |
|---|---|---|---|
| $E_0$ | 24000 Mpa | $\overline{\sigma}_{0T}$ | 2206.9 Mpa |
| $\upsilon$ | 0.2 | $\overline{\sigma}_{90T}$ | 137.9 Gpa |
| $f_t$ | 4.35 Mpa | Fiber volume | 60 % |
| $f_c$ | 46.4 Mpa | 3-ply thickness | 0.4953 mm |
| $\sigma_t$ | 39.5 Mpa | $\rho$ | 1577.25 kg/m$^3$ |
| $\rho$ | 1892.7 kg/m$^3$ | | |

Table 1. Concrete and CFRP material model parameters

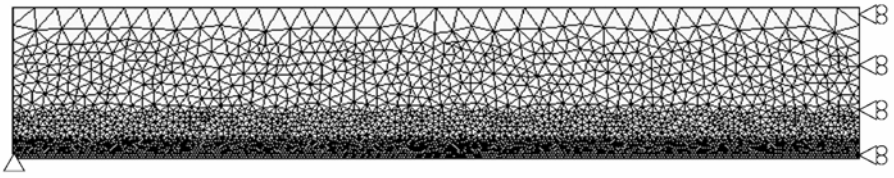

Figure 3. Finite element mesh and boundary conditions

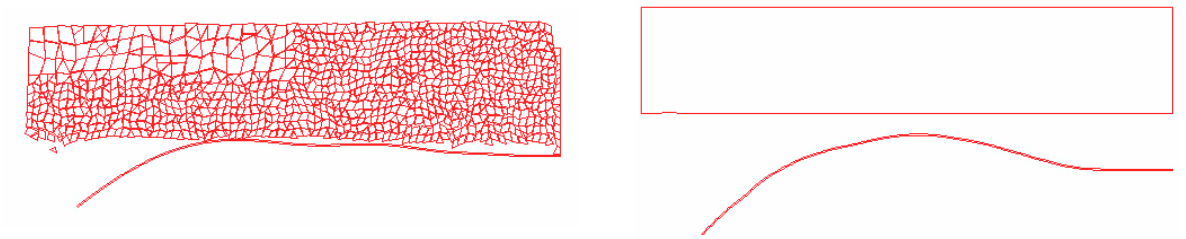

Figure 4. Unrealistic delamination predictions due to incorrect contact (interface) parameters.

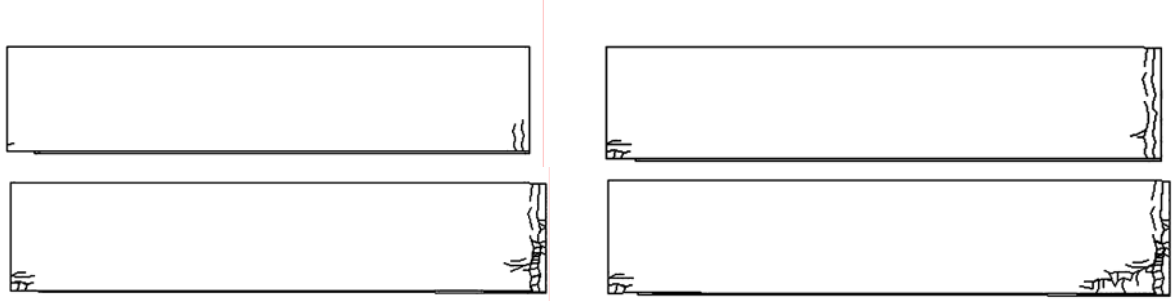

Figure 5. Cracking Pattern at time step=.00046s, .00075s, .000165s, .00174s.

According to the present numerical results, at 0.00113s distinct cracks began to attach to each other. Later, at 0.00127s some signs of delamination were observed at bottom of the beam and at 0.00132 s delamination started to develop gradually. At 0.00136, flexural cracks attached to each other at middle of the beam, while at 0.00145s, more cracks were appeared. At 0.00165s microcracks started to develop from about mid height of the beam toward the left side. Propagation of these cracks increased, so that at 0.00171 s they reached to bottom of the beam and it finally created a complete flexural cracking beside microcracks at bottom of the beam. It is notable that the location where cracks stopped is exactly the same location where delamination of CFRP sheets stopped. It can be seen from the results that the creation and propagation of cracks have occurred at the peak point of the loading.

**3D Modeling**

8-noded cubic elements were used for modeling of the FRP sheet and concrete beam. Similar to 2D simulation, the size of elements were gradually increased for the concrete beam by their distance from bottom of the beam by an increasing ratio of $0.7^{-1}$. No contact interface elements were used for modeling the adhesive layer and instead the contact of adjacent elements was conducted by a node to face contact approach. 1200 and 630 elements were used for modeling the concrete beam and CFRP sheets, respectively.
Again, improper setting of the interface contact related parameters produces unrealistic delamination patterns as depicted in Figure 6. Figures 7 show the debonded region of CFRP sheet from mid span at 470 $\mu s$ and 750 $\mu s$. Maximum principle stress contour at 750 $\mu s$ is illustrated in Figure 8.

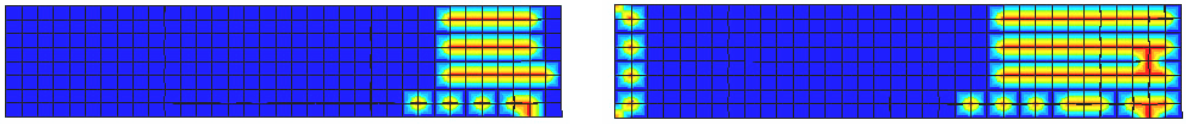

Figure 6. Unrealistic 3D interface debonding patterns.

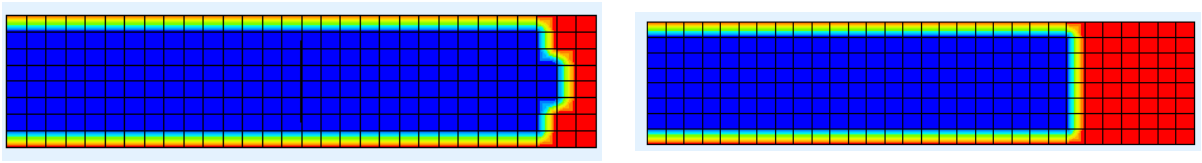

a) time=.00047 s b) time=.00075 s

Figure 7. Delamination growth at different time steps

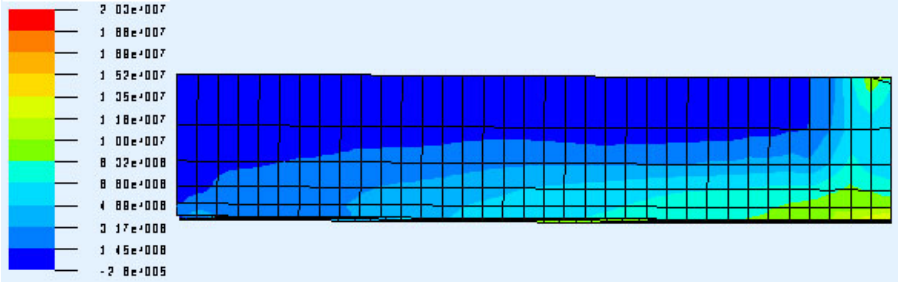

Figure 8. Contour of maximum principle stress at time step=.00075 s

Delamination of CFRP sheet from the concrete beam was approximately started at 470 μs at middle of the beam and propagated toward the support. At 750 μs about one fifth of the total length of FRP sheet was debonded from bottom of the beam as illustrated in Figures 7. As it is observed from Figure 8 the maximum principle stress has exceeded from the tensile strength of concrete in the middle part of the beam which is an indication of occurrence of flexural cracking. The extent of delamination in interlaminar layer to one-fifth of the length of FRP sheets beside the excess of principle stress from the tensile strength of concrete occurs at 750 $\mu s$ which is closely similar to the experimental observations where failure of the beam was reportedly occurred at 730 $\mu s$.
Various displacement history curves at mid span of the beam, computed in different 2D and 3D simulations, were compared to the displacement history resulted from the experimental tests, as depicted in Figure 9. The existing differences can be attributed to the fact that the simulated beam has more stiffness than the tested beam which is a consequence of elastic behavior of concrete in tensile regime without any tensile fracture.

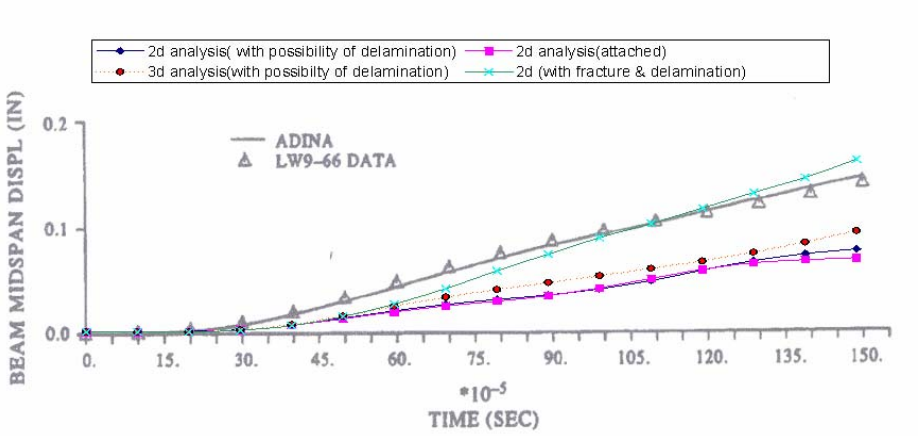


Figure 9. Comparision of mid point displacement vs. time for different solutions

## CONCLUSION

A dynamic debonding model has been proposed based on the finite/discrete element analysis approach for modelling FRP reinforced concrete beams. A mixed coupling model for simulation of delamination of FRP sheet from concrete was developed based on the Hashin criterion. The proposed approach adopts a node to face contact based delamination control to simulate the linear-FRP-RC interactions. Conducting analyses in 2D and 3D and comparing the results with the test results showed that flexural cracking continued by delamination of FRP sheet from mid span is a major failure mode of the beam under dynamic/impact loading. In 3D analysis considerable difference in displacements show that assuming a suitable fracture model for concrete is indispensable for true prediction of overall behavior and failure mode. Close agreement between test results and performed analysis shows that the proposed algorithm may affectively be used for such applications.

## REFERENCES


Arduini M, Tommas AD, Manfroni O. 1995. Fracture mechanism of concrete beams bonded with composite plates. In Taerwe L (ed.), Non-metalic (FRP) reinforcement for concrete structures: 484-91. E&FN Spon: RILEM.

Jerome DM & Ross CA. 1997. Simulation of the dynamic response of concrete beams externally reinforced withcarbon-fiber reinforced plastic. Comput struct 64(5/6): 1129-53.

Klaiber, F.W., Dunker,K.F., Wip, T.J., and Sanders, W.W.,Jr., Methods of strengthening existing highway bridges, NCHRP research report No. 293,Transportation research board, Sep. 1987:11.

Ladner, M. & Weder, C.. Geklebt Bewhrung im Stahlebetonbau, Report No. 206,1981. EMPA Dubendorf Meier, U.. Bridge repair with high performance composite materials. Material Tech, 1978, Vol. 4: 125-128.

Mohammadi S. 2003. Discontinuum mechanics Using Finite and Discrete Elements. WIT Press, UK.

Nishida H, Kamiharako A, Shimomura T, Maruyama K. 1999. Bond mechanism between continuous fiber and concrete. Proc JCI 21(3): 1507-12.

Rahimi R & Hutchinson A. 2001. Concrete beams strengthening with externally bonded FRP plates. ASCE J Compos Constr 5(1):44-56.

Taljsten B. 1996. Strengthening of concrete prisms using the plate-debonding technique. Int J Fract 81:253-66.

Teng JG, Chen JF, Smith ST, Lam L. 2002. FRP strengthened RC structures. Chichester: John Wiley and Sons.

Yuan H, Wu ZS, Yoshizawa H. 2001. Theoretical solution on interfacial stress transfer of externally bonded steel/composite laminates. J Struct Mech Earthquake Eng JSCE 4:27-39.

Zhang S, Raoof M, Wood LA. 1997. Prediction of peeling failure of reinforced concrete beams with externally bonded plates. Proceedings of the Institution of Civil Engineers.Struct Build 122:493-6.

Zhishen Wu & Jun Yin. 2003. Fracturing behaviors of FRP-strengthened concrete structures. Eng Fract Mech 70: 1339-1355.

Ziraba YN. 1995. Computational model for reinforced concrete beams strengthened by epoxy bonded steel plates. Finite Elem Anal Des 12(4): 203-19.